Journal of Molecular Spectroscopy **198,** 115–122 (1999)
Article ID jmsp.1999.7947, available online at http://www.idealibrary.com on IDEAL®

Direct High-Resolution Determination of the Singlet–Triplet Splitting in NH Using Stimulated Emission Pumping

Jan Leo Rinnenthal and Karl-Heinz Gericke

Institut für Physikalische und Theoretische Chemie, Technische Universität Braunschweig, Hans-Sommer-Strasse 10, D-38106 Braunschweig, Germany

Received April 29, 1999; in revised form July 23, 1999

A completely resolved spectrum of the strongly forbidden NH ($a^1\Delta \rightarrow X^3\Sigma^-$) transition is observed. The NH radicals in the excited $a^1\Delta$ state are exclusively generated in a Nd:YAG laser photolysis of hydrazoic acid at a wavelength of 266 nm. The NH ($a^1\Delta \rightarrow X^3\Sigma^-$) intercombination transition around 794 nm is used to produce NH ($X^3\Sigma^-$) applying the stimulated emission pumping technique. The ground state radicals are detected by laser-induced fluorescence (LIF). The energy splitting between the NH ($X^3\Sigma^-$, $v = 0$, $J = 1$, $N = 0$) state and the NH ($a^1\Delta$, $v = 0$, $J = 2$) state is determined with an accuracy of 0.1 cm^{-1} to $\Delta E = 12\ 687.8_{65}$ cm^{-1}. In addition, the radiative lifetime τ of the NH ($a^1\Delta \rightarrow X^3\Sigma^-$) transition was estimated by a determination of the saturation intensity to be $\tau \approx 12.5$ s.

INTRODUCTION

The NH radical was already known for a very long time and was the subject of numerous investigations. It plays an important role in combustion processes when nitrogen-containing fuels are heated before entering the combustion zone because thermal decomposition occurs and produces low molecular weight compounds including NH (*1, 2*). Furthermore, it is an important astrochemical species having been observed in the spectra of comets (*3*) and stars (*4*).

Already in 1893, Eder examined the NH ($A^3\Pi \leftrightarrow X^3\Sigma^-$) band system at 336 nm (*5*). In the 1930s, Funke was the first who assigned the main branches of the strong (0–0) and (1–1) bands of this transition (*6*). He also reported details about the Λ and spin splitting of the observed bands. In 1959, Dixon improved the analysis of this band system by the observation of lines from most of the satellite branches. He was able to identify the lines which could be attributed to 25 branches of the (0–0) band and 19 branches of the (1–0) band (*7*). The analysis of the (0–0) band led to a correction of the line assignments previously published by Funke for this band. Dixon considered the spin splittings in both the *A* and *X* electronic states and the Λ doubling in the *A* state in detail and obtained reasonably accurate rotational and fine structure constants. The weaker (0–1), (1–2), (1–0), and (2–1) bands were studied by Malicet *et al.* (*8*). In 1986, Brazier *et al.* used a Fourier transform spectrometer with a precision of ± 0.0002 cm^{-1} for the strong unblended lines in the (0–0) band. This improved the accuracy of the measurements by more than two orders of magnitude (*9*). In 1999, the values were improved again (*10*).

In the 1930s, the NH radical was also observed in its singlet states via the NH ($c^1\Pi$, $v = 0 \rightarrow a^1\Delta$, $v = 0$) transition around 324 nm by three independent groups at nearly the same time (*11–13*). After Ramsay and Sarre analyzed the (0–1) band of this transition (*14*), the hyperfine and Λ-doubling constants were observed in a molecular beam experiment by Ubachs *et al.* (*15*). Transitions connecting to either $c^1\Pi$ or $a^1\Delta$ like NH ($d^1\Sigma^+ \leftrightarrow c^1\Pi$) (*16, 17*) and NH ($c^1\Pi \leftrightarrow b^1\Sigma^+$) (*18*) were also recorded.

Despite the large amount of spectroscopy work on the NH radical, the singlet–triplet splitting was still unknown until 1974 when Masanet *et al.* recorded the NH ($b^1\Sigma^+ \leftrightarrow X^3\Sigma^-$) transition to the ground state in a VUV gas-phase photolysis experiment of HN_3. A few years later, Cossart improved the resolution for this transition (*19*). Rohrer and Stuhl observed the NH ($a^1\Delta \rightarrow X^3\Sigma^-$) transition directly (*20*).

In the present work, all lines of the strongly forbidden NH ($a^1\Delta \rightarrow X^3\Sigma^-$) transition are resolved for the first time and the singlet–triplet splitting of the NH radical is determined with a significantly improved accuracy. Furthermore, the first experimental value for the radiative lifetime in the gas phase is given.

Three different steps are involved in this experiment. In the first step, NH ($a^1\Delta$) is generated in a Nd:YAG laser photolysis of hydrazoic acid (HN_3) at a wavelength of 266 nm. In the second step, intense tunable laser light in the wavelength region around 790 nm is used to stimulate the NH ($a^1\Delta \rightarrow X^3\Sigma^-$) transition after complete translational and rotational relaxation within the $a^1\Delta$ state has occurred. In the third step, the generated NH ($X^3\Sigma^-$) radicals are detected by laser-induced fluorescence (LIF) using the NH ($A^3\Pi \leftarrow X^3\Sigma^-$) transition. Analogously to the stimulated emission (dump) step, this is performed after complete rotational relaxation in the $X^3\Sigma^-$ state. By means of this technique, the extremely weak NH ($a^1\Delta \rightarrow X^3\Sigma^-$) transition can be amplified due to induced processes and thereby be recorded with a spectral resolution

0022-2852/99 $30.00

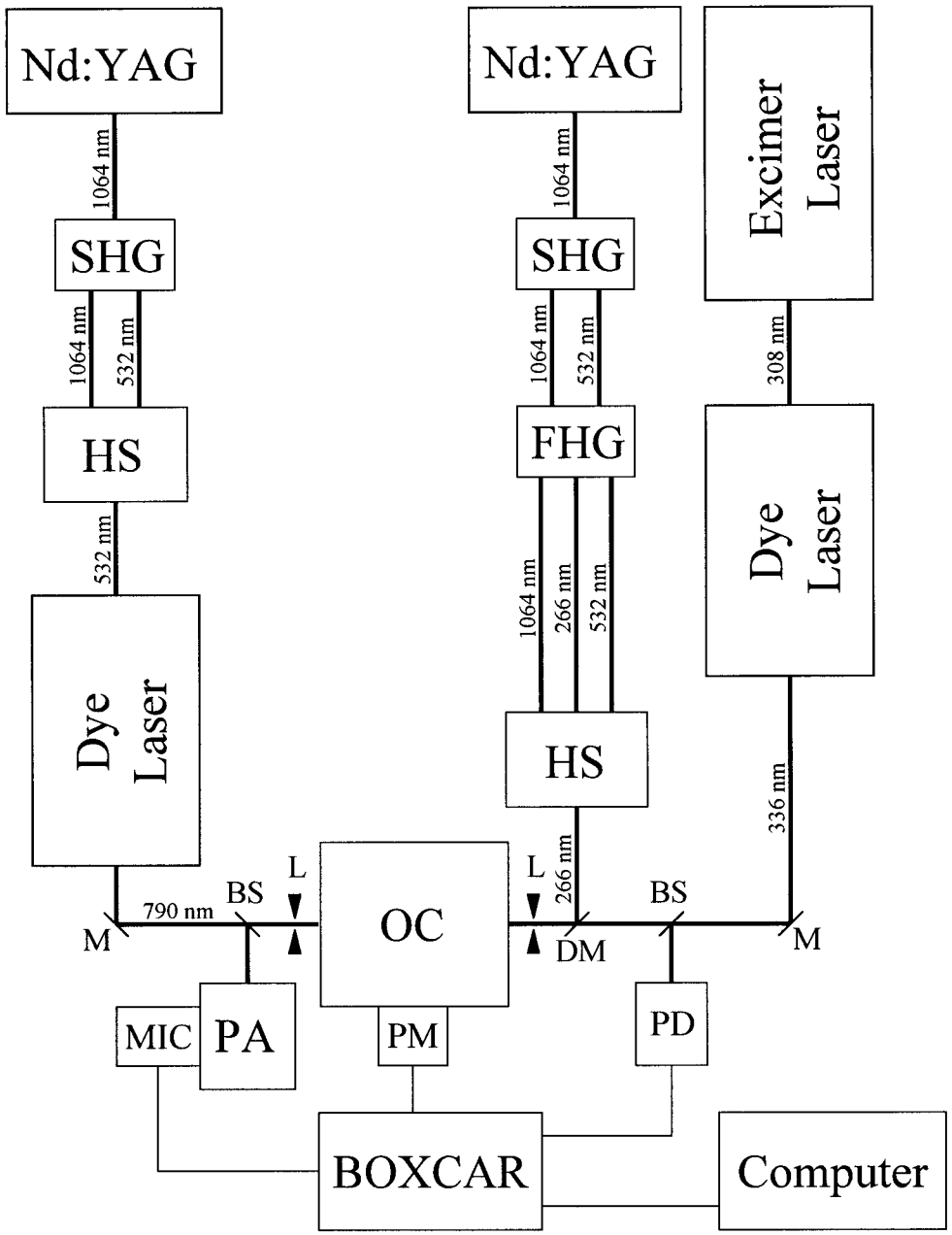

FIG. 1. Schematic picture of the experimental setup. (SHG = second harmonic generator, FHG = fourth harmonic generator, HS = harmonic separator, OC = observation chamber, M = mirror, DM = dichroitic mirror, BS = beam splitter, L = lens, MIC = microphone, PA = photoacoustic cell, PM = photomultiplier, PD = photodiode.)

that is only limited by the Doppler width if the bandwidth of the dump laser is negligible.

EXPERIMENT

Figure 1 shows the experimental setup. The precursor of the NH radical is hydrazoic acid, HN_3, which is generated by heating a mixture of sodium azide, NaN_3, and stearic acid under vacuum conditions. At about 85°C, the only evolving gas is HN_3, which is stored in a glass bulb at a maximum pressure of about 1 kPa (*21*). Alternatively, HN_3 can also be prepared by adding small amounts of phosphoric acid under vacuum to NaN_3, which is much simpler to handle, but the generated HN_3 is less pure (*22*). The pressure in the glass bulb is monitored by a capacitance pressure transducer (MKS Baratron 221AHS-D-100). To achieve a sufficiently fast rotational relaxation of NH ($a^1\Delta$), HN_3 is diluted by known amounts of Ne in a second glass bulb. The appropriate mixing ratio is

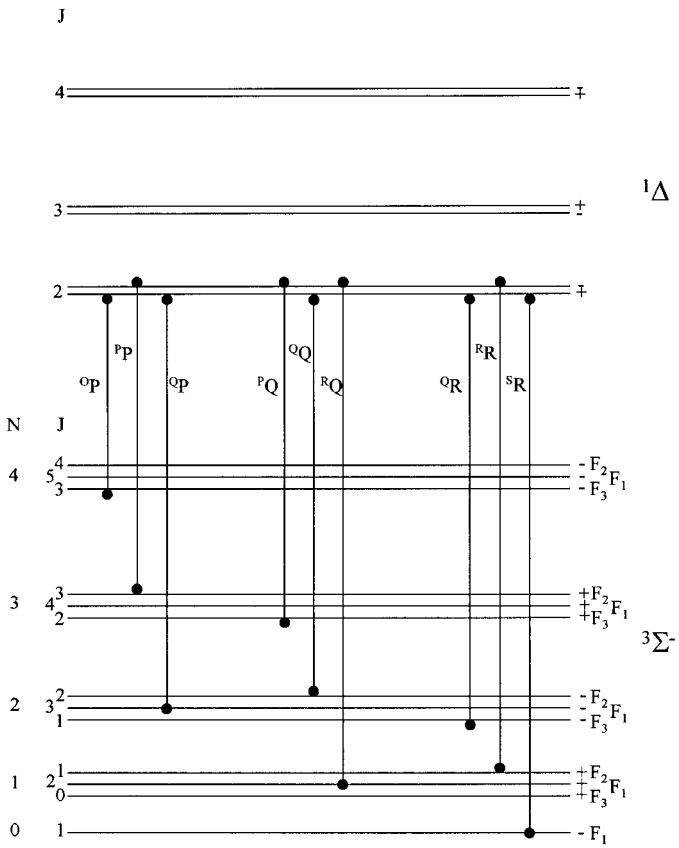

FIG. 2. Energy level diagram and all connecting branches of the ($a^1\Delta \rightarrow X^3\Sigma^-$) system. $^SR(1)$ (0,0) = singlet–triplet splitting.

about HN_3:Ne = 1:10^5 up to 1:10^4 if the total pressure in the observation chamber is about 10^4 Pa. These conditions provide sufficient NH ($X^3\Sigma^-$) probe signal intensity and at the same time avoid electronic quenching of NH ($a^1\Delta$) by HN_3 (*23, 24*).

An oil diffusion pump reaching a base pressure of $\sim 10^{-2}$ Pa evacuates the observation chamber. The total pressure in the chamber is measured using a second capacitance pressure transducer (MKS Baratron 221AHS-D-100).

NH ($a^1\Delta$) is generated in a pulsed photodissociation of HN_3 by a light pulse of 30 mJ at 266 nm generated by the fourth harmonic of a Nd:YAG laser (Continuum Surelite II-10). At 266 nm, NH is produced exclusively in its first excited singlet state $a^1\Delta$ (*25*). The experimental results concerning the nascent vibrational distribution of NH ($a^1\Delta$) are not entirely consistent with one another (*26–28*). The latest reported values are ($v = 0$):($v = 1$):($v = 2$) = (1):(0.3):(0.02) (*29*). By adjusting the total pressure in the observation chamber and the HN_3:Ne mixing ratio, the collision rate was chosen such that the rotational distribution is completely relaxed to a Boltzmann distribution at room temperature.

As the Franck–Condon factors for the $\Delta v = v'-v'' = 0$ transitions are close to one and the $v = 0$ vibrational level is the most populated one, the NH ($a^1\Delta$, $v = 0 \rightarrow X^3\Sigma^-$, $v = 0$) transition is used for state-selective stimulated emission pumping to the ground state. This is performed by a Nd:YAG pumped dye laser (Continuum YG 680, TDL 60, IRP) with a pulse width of typically 7 ns and a bandwidth (FWHM) of 0.08 cm^{-1}. Because of saturation effects, at a pulse energy of 30 mJ the effective bandwidth increased to about 0.2 cm^{-1}. The wavelength range 770–830 nm was covered by the laser dyes LDS 765 and 821.

A photoacoustic cell is used to calibrate the wavelength of the analyzing dump laser with high accuracy by scanning the (004) ← (000) overtone excitation band of HCN which is in the same wavelength region (*30–33*).

TABLE 1
Hönl–London Factors of ($a^1\Delta \rightarrow X^3\Sigma^-$) Transitions (*37*)

branch	Hönl-London factor
$^OP(J)$	$\frac{(J-2)(J-1)}{4(2J+1)}$
$^PP(J)$	$\frac{(J-2)(J-1)}{4J}$
$^QP(J)$	$\frac{(J-2)(J-1)(J+1)}{4J(2J+1)}$
$^PQ(J)$	$\frac{(J-1)(J+2)}{4(J+1)}$
$^QQ(J)$	$\frac{(J-1)(J+2)(2J+1)}{4J(J+1)}$
$^RQ(J)$	$\frac{(J-1)(J+2)}{4J}$
$^QR(J)$	$\frac{J(J+2)(J+3)}{4(J+1)(2J+1)}$
$^RR(J)$	$\frac{(J+2)(J+3)}{4(J+1)}$
$^SR(J)$	$\frac{(J+2)(J+3)}{4(2J+1)}$

TABLE 2
Spectroscopic Constants Used for the $^1\Delta$ State of NH

	v=0	v=1	Ref.
T	12654.9_{94} cm^{-1}	15837.$_{91}$ cm^{-1}	this work
B	16.432551(76) cm^{-1}	15.814214(87) cm^{-1}	(*42*)
D	16.7309(57) $\times 10^4$ cm^{-1}	16.4156(69) $\times 10^4$ cm^{-1}	(*42*)
H	11.54(22) $\times 10^8$ cm^{-1}	11.01(24) $\times 10^8$ cm^{-1}	(*42*)
q	-4.82(31) kHz		(*14*)

Note. Values in parentheses represent the standard deviation in the last digits.

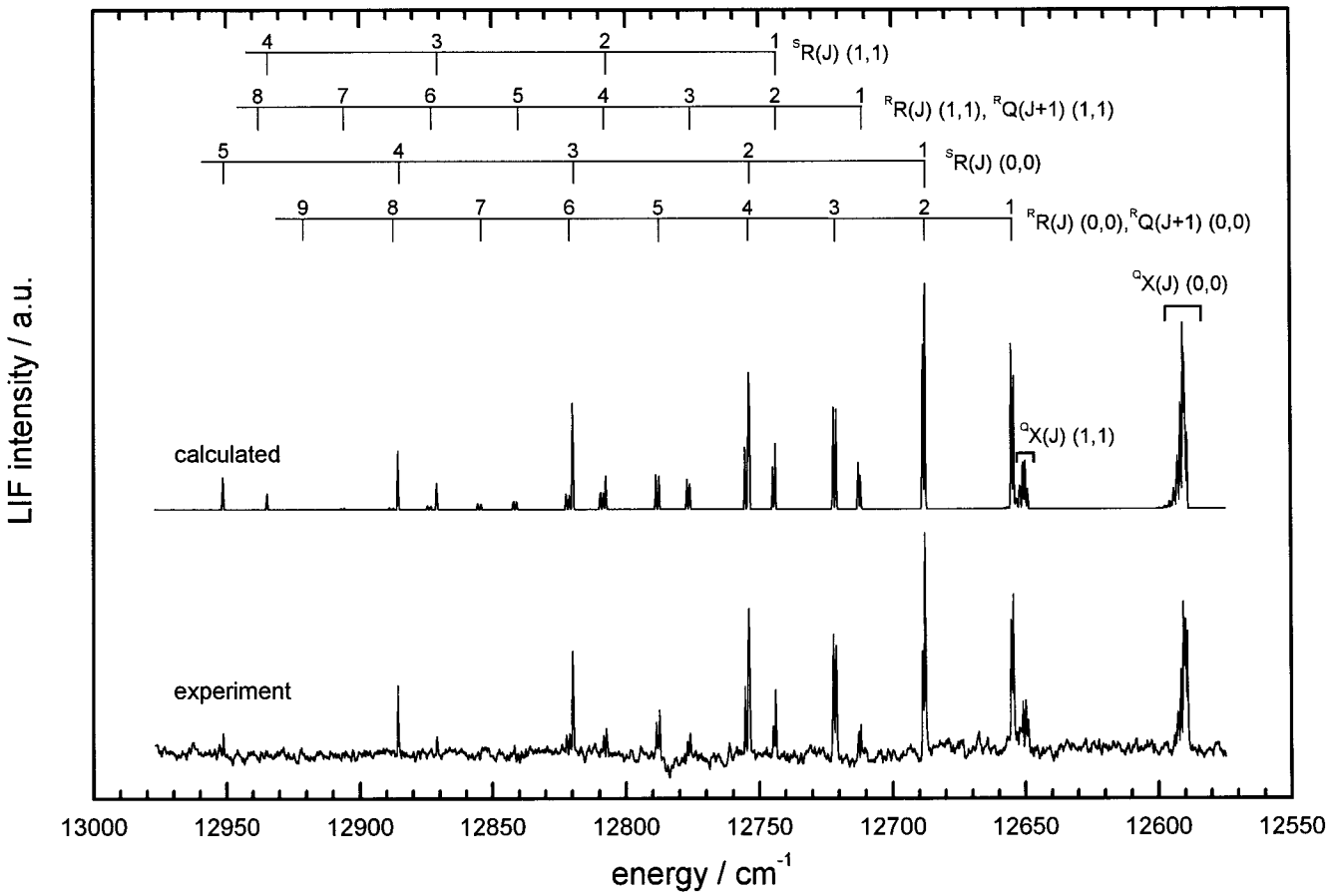

FIG. 3. ${}^{S}R(J)$, ${}^{R}R(J)$, ${}^{R}Q(J)$, ${}^{Q}P(J)$, ${}^{Q}Q(J)$, and ${}^{Q}R(J)$ branches of the high-resolution spectrum of the forbidden ($a^1\Delta \rightarrow X^3\Sigma^-$) transition obtained by scanning the dump laser wavelength. For comparison a calculated spectrum is also shown. The spectral resolution is 0.2 cm^{-1} (FWHM). The singlet–triplet splitting is directly given by the ${}^{S}R(1)$ line. Its value is $\Delta E = 12\,687.8_{65}$ cm^{-1}. The rotational temperature is 300 K. The delay between the photolysis and the dump pulse is 100 ns and the probe laser is further delayed by 500 ns. The pressures are 10^4 Pa Ne and 0.1 Pa HN_3.

The rotationally relaxed NH ($X^3\Sigma^-$) radicals are detected by applying the laser-induced fluorescence (LIF) technique (*34–36*) via the NH ($X^3\Sigma^-$, $v = 0 \leftrightarrow A^3\Pi$, $v = 0$) band. An excimer laser (Radiant Dyes, RD-EXC-200) pumped dye laser (Lambda Physik, FL 3002) supplies the necessary detection wavelength of 337.01 nm which corresponds to the $P_1(2)$ line. This line is chosen because it is a very intense one in a rotational relaxed LIF spectrum. Excitation of NH ($X^3\Sigma^-$) is performed under saturated conditions at a pulse energy of 2 mJ. Total fluorescence is monitored with a photomultiplier (Thorn-EMI 9781B) perpendicular to the probe beam through $f/1$ optics and an interference filter (330 ± 30 nm).

All laser beams are aligned parallel to each other and the stimulated emission laser beam is counterpropagating the photolysis and probe beams (Fig. 1). The photolysis and probe laser beams are focused by 500-mm lenses; for the dump beam, a 300-mm lens is used to increase its intensity because of the extremely low transition probability of the NH ($a^1\Delta$, $v = 0 \rightarrow X^3\Sigma^-$, $v = 0$) transition. To reduce the influence of scattered light, the laser beams were guided through baffles into the observation chamber.

A boxcar integrator (Stanford Research System, DG 535), which is triggered by the probe laser beam via a photodiode, registers and averages the LIF signal. Finally, a computer records the experimental data for further processing.

The time delay between the photolysis laser pulse and the dump laser pulse is set to 100–150 ns. Between the dump laser pulse and the probe laser pulse it is set to 300–500 ns to assure complete rotational relaxation. All lasers operate at a repetition rate of 10 Hz. All trigger pulses are generated by two coupled trigger generators (Stanford Research System DG 535 and a home-built generator).

To align the detection laser exactly to a transition of NH ($A^3\Pi \leftarrow X^3\Sigma^-$), it is necessary to have a source of NH ($X^3\Sigma^-$). For this purpose, NH ($X^3\Sigma^-$) is generated via quenching of NH ($a^1\Delta$) by increasing the delay time between photolysis laser pulse and detection laser pulse up to 200 μs.

The following conditions have to be fulfilled in the experiments.

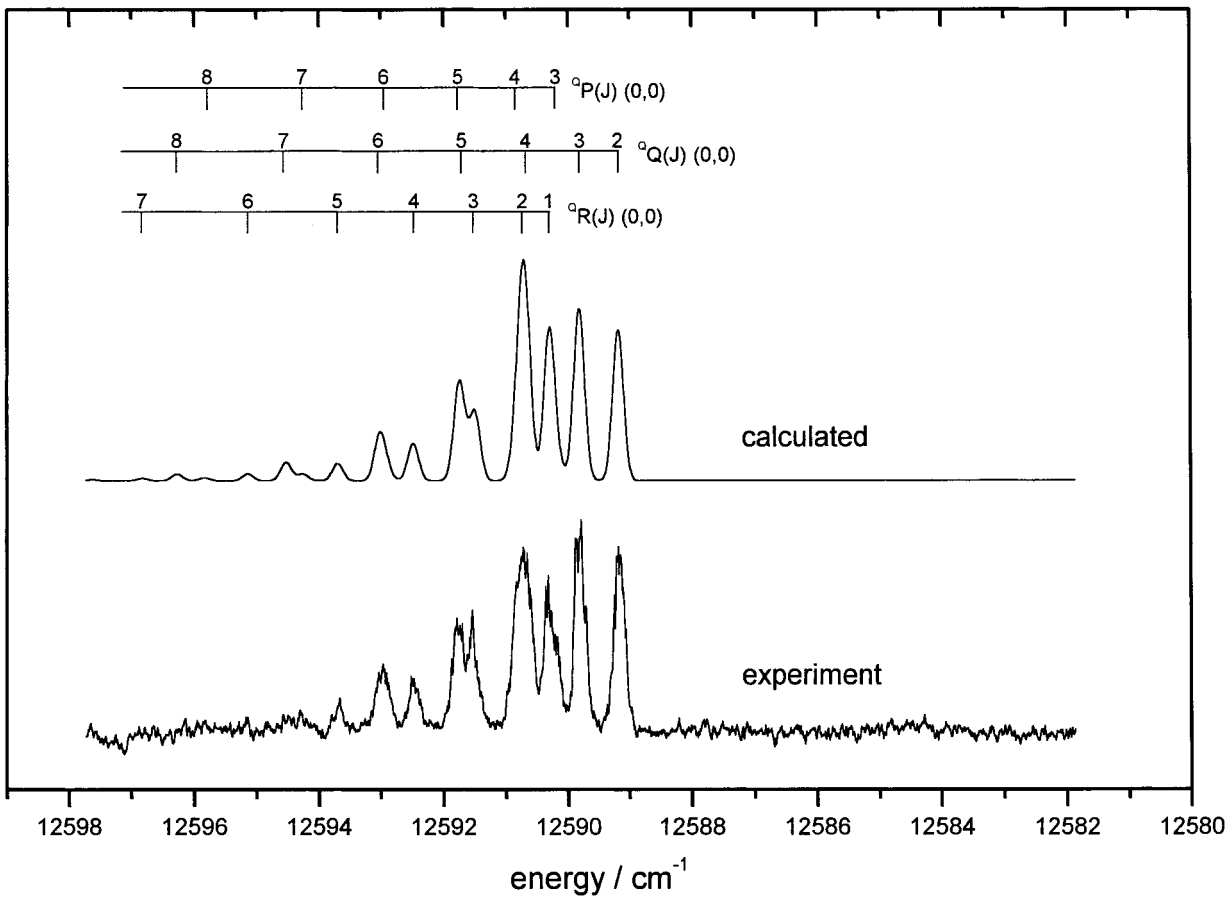

FIG. 4. Blowup of the experimentally observed $^{Q}P(J)$, $^{Q}Q(J)$, and $^{Q}R(J)$ branches of the forbidden ($a^1\Delta \rightarrow X^3\Sigma^-$) transition and the calculated spectrum. The spectral resolution is 0.2 cm^{-1} (FWHM); the rotational temperature is 300 K. Experimental conditions as indicated in Fig. 3.

1. There has to be a strong population inversion between the triplet and the singlet state. In the photodissociation of HN_3 at 266 nm, the inversion is 100% directly after the photolysis laser pulse because no ground state radicals are produced ($P(a^1\Delta)/P(X^3\Sigma^-) \rightarrow \infty$).

2. Complete rotational relaxation has to be significantly faster than electronic quenching. If the rotational distribution in the NH ($X^3\Sigma^-$) state is not relaxed before the LIF detection, then the dump spectrum might be incomplete.

RESULTS AND DISCUSSION

A ($a^1\Delta \rightarrow X^3\Sigma^-$) transition consists of nine branches which are denoted as $^{\Delta N}\Delta J(J)$, where ΔN represents the change of the nuclear rotation quantum number N, whereas ΔJ represents the change of the total angular momentum quantum number J. Thus, the branches $^{O}P(J)$, $^{P}P(J)$, $^{Q}P(J)$, $^{P}Q(J)$, $^{Q}Q(J)$, $^{R}Q(J)$, $^{Q}R(J)$, $^{R}R(J)$, $^{S}R(J)$ can be expected (*37*). Figure 2 represents an energy level diagram with all branches and Table 1 lists the corresponding Hönl–London factors of each branch. All Hönl–London factors are normalized to $2J + 1$.

The energy levels of NH ($X^3\Sigma^-$) are directly taken from Ref. (*9*) because of their high accuracy. The energy levels of NH ($a^1\Delta$) can be calculated with a sufficient accuracy using the following formulas:

$$T(e,v,J,\delta) = T_v + F(v,J,\delta) \quad [1]$$

$$F(v,J,\delta) = B_v(J(J+1) - \Lambda^2) - D_v(J(J+1) - \Lambda^2)^2 + H_v(J(J+1) - \Lambda^2)^3 + \Delta E_\delta(J) \quad [2]$$

$$\Delta E_\delta(J) = \delta \cdot q(J-1)J(J+1)(J+2), \quad [3]$$

where $\delta = 1$ if parity $= (-1)^J$ and $\delta = 0$ if parity $\neq (-1)^J$ and $\Lambda = 2$.

$T(e,v,J,\delta)$ is the energy of a rovibrational state, T_v is the vibrational energy including the electronic energy of the $^1\Delta$ state, $F(v,J,\delta)$ is the rotational energy, B_v, D_v, and H_v are the rotational constants, $\Delta E_\delta(J)$ represents the Λ splitting, and q is the Λ-splitting constant. The constants used for the simulation are listed in Table 2.

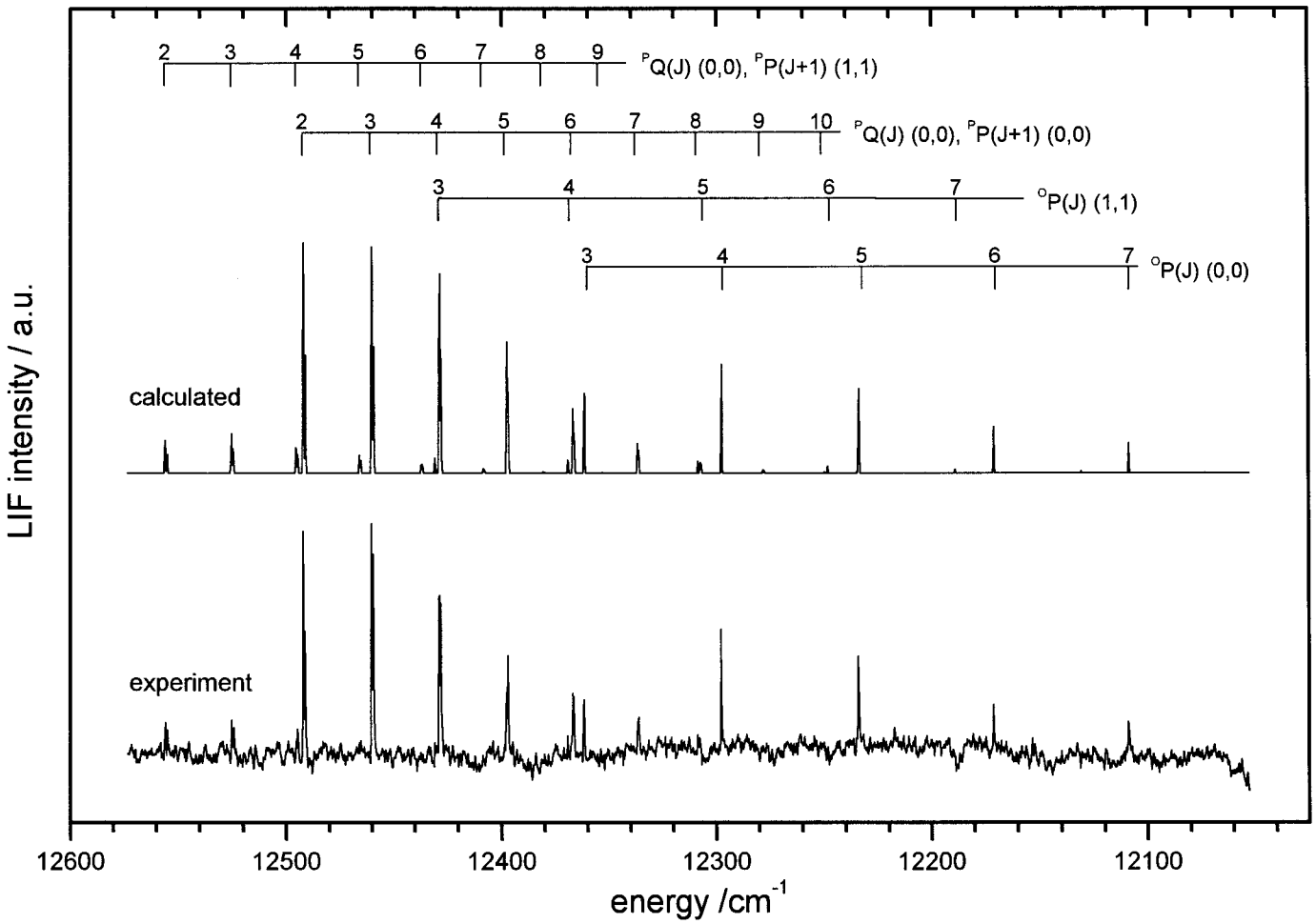

FIG. 5. Observed ${}^{P}Q(J)$, ${}^{P}P(J)$, and ${}^{O}P(J)$ branches of the $(a^1\Delta \rightarrow X^3\Sigma^-)$ transition and calculated spectrum. The spectral resolution is 0.2 cm^{-1} (FWHM) and the rotational temperature is 300 K. The delay between the photolysis and the dump pulse is 150 ns and the delay between the dump pulse and the probe pulse is 300 ns. The pressures are as indicated in Fig. 3.

For the calculation of the spectrum, the line positions of each rovibrational transition and its intensities were computed. The lineshapes were assumed to be Gaussian and are represented by

$$I(\nu) = I_0 e^{-4\ln 2((\nu-\nu_0)/\Delta\nu)^2} \qquad [4]$$

with $\Delta\nu$ = FWHM.

The line positions are given by subtracting the energy of the levels corresponding to each line of the nine branches. If no saturation occurs, the intensity I of each rovibrational line is

$$I \propto P(v,J) \cdot FC(v) \cdot \frac{HL(J)}{(2J+1)}, \qquad [5]$$

where $FC(v)$ and $HL(J)$ are the Franck–Condon and Hönl–London factors (Table 1) and $P(v,J)$ is the population of the initial rovibrational state. The Franck–Condon factors for the $(\Delta v = 0)$ transitions are all close to one (*38*).

If the transition is saturated, the Hönl–London factor is replaced by a factor

$$g_S = \frac{g(J')}{g(J'') + g(J')}, \qquad [6]$$

where $g(J'')$ and $g(J')$ represent the degeneracies of the $(a^1\Delta)$ and the $(X^3\Sigma^-)$ state, respectively.

The intensity distribution which fits best the experimental data is calculated by assuming an intermediate case (nearly saturated). Therefore, the line intensities were calculated by adding the intensities of both cases with appropriate weight. As explained below, this fact can be used to determine the absorption cross section and, as a consequence, the radiative lifetime.

Figure 3 shows the recorded and the calculated spectrum of the branches ${}^{S}R(J)$, ${}^{R}R(J)$, ${}^{R}Q(J)$, ${}^{Q}P(J)$, ${}^{Q}Q(J)$, and ${}^{Q}R(J)$. All lines are represented by the vibrational transitions $(0 \rightarrow 0)$ and $(1 \rightarrow 1)$. Figure 4 shows a blowup of the ${}^{Q}P(J)$, ${}^{Q}Q(J)$,

and ${}^{Q}R(J)$ branch for the vibrational transition $(0 \rightarrow 0)$. Finally, in Fig. 5 the branches ${}^{P}Q(J)$, ${}^{P}P(J)$, and ${}^{O}P(J)$ are shown. All spectra represent a rotational temperature of 300 K that is consistent with the expected value because of the chosen delay time between dissociation and stimulated emission of 100–150 ns. Thus, all recorded spectra are fully rotationally relaxed.

The ${}^{S}R(1)(0 \rightarrow 0)$ line in Fig. 3 directly gives the energy splitting between the lowest NH ($X^3\Sigma^-$, $v = 0$, $J = 1$, $N = 0$) state and the lowest NH ($a^1\Delta$, $v = 0$, $J = 2$) state (singlet–triplet splitting). A least-squares fit of $T_{v=0}$ results in a value of $12\,654.9_{94}$ cm^{-1}. This corresponds to a value of $\Delta E = 12687.8_{65}$ cm^{-1} for the singlet–triplet splitting. Our new value improves the old one (12 688.39 cm^{-1}) given by Ram and Bernath (*39*). The accuracy of the fit is 0.01 cm^{-1}. However, we estimate an accuracy of 0.1 cm^{-1} due to the calibration accuracy of the dump laser. To determine the absolute line position, a photoacoustic cell (PA; Fig. 1) was used to calibrate the stimulated emission laser by recording a photoacoustic spectrum of the (004)←(000) overtone band of HCN, which lies in the same wavelength region as the NH spectrum. The laser calibration was optimized by scanning over the $P(4)$ line at 12 623.538 cm^{-1} (*30*), yielding an accuracy of less than 0.1 cm^{-1}.

In general, the radiative lifetime τ of NH ($a^1\Delta$) is determined by saturating the dump transition. For a transition from state n to state m, τ_{nm} is related to the total absorption cross-section σ_{tot} via the equation

$$\tau_{nm} = \frac{1}{A_{nm}} = \frac{c^2}{8\pi\nu_{nm}^2\sigma_{\text{tot}}}, \qquad [7]$$

which is obtained by the well-known relation between the probability for stimulated emission $B_{nm} = (c/h\nu)\sigma_{\text{tot}}$ and for spontaneous emission A_{nm}. c is the speed of light; ν_{nm} is the frequency of the $n \rightarrow m$ transition. For $\Delta\nu_{\text{laser}} > \Delta\nu_{\text{D}}$, the total cross-section σ_{tot} is related to the differential cross-section σ_d

$$\sigma_{\text{tot}} = \sigma_d \Delta\nu_{\text{laser}} \frac{(2J+1)}{\text{HL}(J)}, \qquad [8]$$

where $\Delta\nu_D$ is the Doppler width, $\Delta\nu_{\text{laser}}$ is the laser linewidth (FWHM), σ_d is the differential cross section, and $\text{HL}(J)$ is the Hönl–London factor of the considered line.

As mentioned above, the recorded spectrum at laser photon flux I_{laser} was nearly saturated:

$$\sigma_d \cdot I_{\text{laser}} \approx 1. \qquad [9]$$

To quantify this intensity, the focus area must be calculated. For a laser beam with Gaussian intensity distribution, wavelength λ, and beam diameter d, the beam cross-section A in the focus is

$$A = \frac{4\lambda^2 M^4 f^2}{\pi d^2} \qquad [10]$$

with $M = \Theta/\theta$, where $\theta = 4\lambda/(\pi d)$ is the beam divergence caused only by diffraction and Θ is the real beam divergence. In the present experiment, a value of $M = 1.1$ is determined yielding a focus area of $A = 6.6 \cdot 10^{-3}$ mm and a focus diameter of 92 μm. This corresponds to a photon flux $I_{\text{laser}} = 1.8 \cdot 10^{21}$ cm^{-2} resulting in a total cross section of $\sigma_{\text{tot}} = 2.01 \cdot 10^{-11}$ cm^2/s for the ${}^{Q}Q(2)$ line (Eq. [9], [8]). According to Eq. [7], we obtain a radiative lifetime of $\tau \approx 12.5$ s. This result is in agreement with the theoretically estimated values of Yarkony ($\tau = 2.18$ s) (*40*) and Marian *et al.* ($\tau = 1.7$ s) (*41*). A lower limit $\tau = 3.3$ s and $\tau = 1.9$ s was previously obtained from extrapolating matrix data (*42, 43*), which supports our directly determined value.

ACKNOWLEDGMENTS

Support of this work by the Deutsche Forschungsgemeinschaft and Fonds der Chemischen Industrie is gratefully acknowledged.

REFERENCES

1. I. Glassman, "Combustion," Academic, New York, 1977, p. 219.
2. G. B. Debrou, J. M. Goodings, and D. K. Bohme, *Combust. Flame* **39,** 1 (1980).
3. M. M. Litvak and E. N. Rodriquez Kuiper, *Astrophys. J.* **253,** 622 (1982).
4. D. L. Lambert, J. A. Brown, K. A. Hinkle, and H. R. Johnson, *Astrophys. J.* **284,** 223 (1984).
5. J. M. Eder, *Denkschr. Wien. Akad.* **60,** 1 (1893).
6. G. W. Funke, *Z. Phys.* **96,** 787 (1935).
7. R. N. Dixon, *Can. J. Phys.* **37,** 1171 (1959).
8. J. Malicet, J. Brion, and H. Guenebaut, *J. Chim. Phys.* **67,** 25–30 (1970).
9. C. R. Brazier, R. S. Ram, and P. F. Bernath, *J. Mol. Spectrosc.* **120,** 381 (1986).
10. R. S. Ram, P. F. Bernath, and K. H. Hinkle, *J. Chem. Phys.* **110,** 5557 (1999).
11. R. W. B. Pearse, *Proc. R. Soc. A* **143,** 112–123 (1934).
12. G. H. Dieke and R. W. Blue, *Phys. Rev.* **45,** 395–400 (1934).
13. G. Nakamura and T. Shidei, *Jpn. J. Phys.* **10,** 5–10 (1934).
14. D. A. Ramsay and P. J. Sarre, *J. Mol. Spectrosc.* **93,** 445 (1982).
15. W. Ubachs, G. Meyer, J. J. ter Meulen, and A. Dymanus, *J. Mol. Spectrosc.* **115,** 88 (1986).
16. W. R. M. Graham and H. Lew, *Can. J. Phys.* **56,** 85 (1978).
17. R. W. Lunt, R. W. B. Pearse, and E. C. W. Smith, *Proc. R. Soc. London Ser. A* **155,** 173 (1936); F. L. Whittaker, *Proc. Phys. Soc. London* **90,** 535 (1967); G. Krishnamurty and N. A. Narasimham, *J. Mol. Spectrosc.* **29,** 410 (1969).
18. R. W. Lunt, R. W. B. Pearse, and E. C. W. Smith, *Proc. R. Soc. London A* **151,** 602 (1935); F. L. Whittacker, *J. Phys. B* **1,** 977 (1968).
19. D. Cossart, *J. Chim. Phys. (Paris)* **76,** 1045 (1979).
20. F. Rohrer and F. Stuhl, *Chem. Phys. Lett.* **111,** 234 (1984).
21. K.-H. Gericke, M. Lock, R. Fasold, and F. J. Comes, *J. Chem. Phys.* **96,** 422 (1992).
22. T. Haas, K.-H. Gericke, and C. Maul, *Chem. Phys. Lett.* **202,** 108 (1993).
23. J. W. Cox, H. H. Nelson, and J. R. McDonald, *Chem. Phys.* **96,** 175 (1985).
24. R. D. Bower, M. T. Jacoby, and J. A. Blauer, *J. Chem. Phys.* **86,** 1954 (1987).

25. F. Rohrer and F. Stuhl, *J. Chem. Phys.* **88,** 4788 (1988).
26. J. R. McDonald, R. G. Miller, and A. P. Baronavski, *Chem. Phys. Lett.* **51,** 57 (1977).
27. J. R. McDonald, R. G. Miller, and A. P. Baronavski, *Chem. Phys.* **30,** 133 (1978).
28. H. H. Nelson and J. R. McDonald, *J. Chem. Phys.* **93,** 8777 (1990).
29. M. Hawley, A. P. Baronavski, and H. H. Nelson, *J. Chem. Phys.* **99,** 2638 (1993).
30. A. M. Smith, S. L. Coy, and W. Klemperer, *J. Mol. Spectrosc.* **134,** 134 (1989).
31. A. M. Smith and U. G. Jorgensen, *J. Chem. Phys.* **87,** 5649 (1987).
32. D. Romanini and K. K. Lehmann, *J. Chem. Phys.* **102,** 633 (1995).
33. D. Romanini and K. K. Lehmann, *J. Chem. Phys.* **99,** 6287 (1993).
34. A. Schultz, H. W. Cruse, and R. N. Zare, *J. Chem. Phys.* **57,** 1354 (1972).
35. J. L. Kinsey, *Annu. Rev. Phys. Chem.* **28,** 349 (1978).
36. W. Demtröder, "Laser Spectroscopy," Springer-Verlag, Berlin, 1982, p. 417.
37. I. Kovacs, "Rotational Structure in the Spectra of Diatomic Molecules," Hilger, London, 1969, p. 181.
38. P. W. Fairchild, G. P. Smith, D. R. Crosley, and J. B. Jeffries, *Chem. Phys. Lett.* **107,** 181 (1984).
39. R. S. Ram and P. F. Bernath, *J. Opt. Soc. Am. B* **3,** 1170 (1986).
40. D. R. Yarkony, *J. Chem. Phys.* **91,** 4745 (1989).
41. C. M. Marian and R. Klotz, *Chem. Phys.* **95,** 213 (1985).
42. H. Esser, J. Langen, and U. Schurath, *Ber. Bunsenges. Phys. Chem.* **87,** 636 (1983).
43. A. Ramsthaler-Sommer, K. E. Eberhardt, and U. Schurath, *J. Chem. Phys.* **85,** 3760 (1986).